Journal of Power Sources 249 (2014) 520–526

Contents lists available at SciVerse ScienceDirect

Journal of Power Sources

journal homepage: www.elsevier.com/locate/jpowsour

Electrochemical performance of a solid oxide fuel cell with an anode based on Cu–Ni/CeO_2 for methane direct oxidation

Aitor Hornés [a,**], María J. Escudero [b,***], Loreto Daza [b], Arturo Martínez-Arias [a,*]

[a] Instituto de Catálisis y Petroleoquímica (CSIC), C/Marie Curie 2, Campus de Cantoblanco, 28049 Madrid, Spain
[b] CIEMAT, Avda. Complutense 22, 28040 Madrid, Spain

HIGHLIGHTS

- Direct methane oxidation over CuNi–CeO_2/YSZ/LSF solid oxide fuel cell.
- Anode prepared by impregnation/infiltration from reverse microemulsion.
- Rather stable performance between 1023 and 1073 K.

GRAPHICAL ABSTRACT

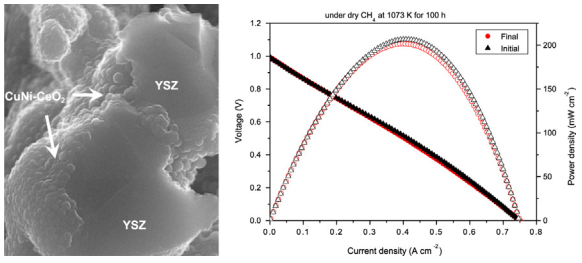

ARTICLE INFO

Article history:
Received 27 December 2012
Received in revised form
27 May 2013
Accepted 30 May 2013
Available online 18 June 2013

Keywords:
CuNi–CeO_2/YSZ/LSF SOFC
Direct CH_4 oxidation
I–V curves
Impedance spectra

ABSTRACT

A CuNi–CeO_2/YSZ/LSF solid oxide fuel cell has been fabricated and tested with respect to its electrochemical activity for direct oxidation of dry methane. The electrodes have been prepared by impregnation of corresponding porous YSZ layers, using reverse microemulsions as impregnating medium for the anode (constituted by Cu–Ni at 1:1 atomic ratio in combination with CeO_2). On the basis of I–V electrochemical testing complemented by impedance spectroscopy (IS) measurements it is shown the ability of the SOFC for direct oxidation of methane in a rather stable way. Differences in the behavior as a function of operating temperature (1023–1073 K) are also revealed and examined on the basis of analysis of IS spectra.

1. Introduction

Solid oxide fuel cells (SOFCs) are galvanic devices which are most interesting from environmental and energetic points of view due to their high efficiency for conversion from chemical to electrical energy and their high versatility toward employment of various types of fuels [1]. Classical systems of this type involve the employment of thin YSZ electrolytes with an anode typically based on Ni-YSZ cermets and can attain an energetic efficiency close to 70% operating at relatively high temperature (1073–1273 K) with hydrocarbon reforming mixtures as fuel [1–3]. This efficiency can be theoretically increased by employing direct hydrocarbon oxidation conditions instead of fuel mixtures resulting from reforming [4,5]. However, the classical nickel anode could easily be deactivated under those conditions as a consequence of the formation of carbonaceous deposits due to the relatively good activity of nickel for hydrocarbon cracking [4,6–8]. Different alternatives were developed in this respect to overcome such deactivation effects. Murray et al. successfully operated a cell on dry methane by employing a nickel-

* Corresponding author. Tel.: +34 915854940; fax: +34 915854760.
** Corresponding author. Present address: German Aerospace Center (DLR), Pfaffenwaldring 38-40, 70569 Stuttgart, Germany.
*** Corresponding author.
E-mail addresses: aitor.hornesmartinez@dlr.de (A. Hornés), m.escudero@ciemat.es (M.J. Escudero), amartinez@icp.csic.es (A. Martínez-Arias).

0378-7753/$ – see front matter © 2013 Elsevier B.V. All rights reserved.
http://dx.doi.org/10.1016/j.jpowsour.2013.05.159

containing ceria-based anode at relatively low reaction temperature (923 K) [6]. In turn, such ceria-containing anode could in principle be compatible with electrolytes able to operate at intermediate temperatures (773–973 K) like gadolinium-doped ceria (CGO) [1].

However, as mentioned, nickel anodes are generally prone to become rapidly deactivated by deposited carbon under direct hydrocarbon oxidation conditions [4,7–10]. A more versatile alternative in this respect was developed by Gorte, Vohs and co-workers and consisted in employing anodes including mixtures between copper and cerium oxide [4,7,10–14]. Such configuration has demonstrated to be able to employ a large diversity of hydrocarbon fuels (methane or longer chain ones and even aromatics) under direct oxidation conditions and displaying a reasonable stability [4,7,12]. Nevertheless, although they could in principle perform well at intermediate temperatures, copper anodes can present several limitations in terms of thermal stability related to its relatively low melting temperature, which can make the fabrication of Cu cermets difficult and affect the anode stability when operating at high temperature, typically above 973 K [4,15,16]; in addition, it must be taken into account the poor performance of copper for hydrocarbon activation [4,9]. An interesting alternative in this sense consists in employing more refractory and catalytically active bi- or multi-metallic anode formulations [4,9,17–19]. Among them, specific formulations of bimetallic Cu–Ni anodes can apparently display promising properties for the process [9,19–21]. Nevertheless, the mentioned higher catalytic activity of nickel toward coke formation can force to employ relatively low Ni/Cu ratios in the formulation while other problems related to mechanical stability as a consequence of such carbon formation which leads to cracking of the cell have also been pointed out [16,22]. Indeed, an important decrease of the power density was observed in a recent report during first hours of operation under methane in the course of durability tests of SOFCs having as anode a combination of Cu–Ni (at about 1:1 atomic ratio) with CGO [21].

In this context, the present work explores the electrochemical properties of a home-made SOFC, having an anode based on combination between Cu–Ni (in 1:1 atomic ratio) and ceria, for direct oxidation of dry methane. The anode was incorporated to the cell by using a method based on impregnation of the components [15]; a novelty here is that reverse microemulsions containing the precursors of the anode components were employed in order to intend to achieve effectively a maximum dispersion and homogeneity within the anode which could lead to optimum nanostructural characteristics [22–26]. In this sense, surfactant assisted infiltration of precursors into a cell was successfully employed by P. Blennow et al. [27], providing good surface coverage of a strontium titanate backbone by nano-sized CGO particles and achieving remarkable cell performance. Characterization of the separate anode formulation similar to the one employed here both in terms of structural properties as well as redox behavior toward interaction with methane has been reported recently [22]. The results here show the promising characteristics in terms of performance and durability of the fabricated SOFC having the mentioned type of anode under pure methane.

2. Experimental

For preparing the fuel cell, a green tape of the electrolyte was first prepared from an aqueous suspension of YSZ (Tosoh-zirconia with 8% Y_2O_3 and 0.2 μm particle size) including a dispersant (Rohm & Haas DURAMAX d-3005) which was agitated for 4 h in a ball mill. It was then left for 24 h more under stirring after addition of solutions of two organic ceramic binders (DURAMAX B-1000 y HA-12). Then, once the dense emulsion achieved the desired weight, a film of about 150 μm thickness was obtained from it by tape casting and was dried for 24 h under atmospheric air at room temperature. The same procedure was employed to deposit porous YSZ layers at both sides of the initial tape for which a pore former (Graphite ALFA; 325 mesh) was added. Then, 20 mm diameter circular wafers were cut with the two porous layers of about 9.5 mm diameter being concentrically disposed. Such wafer was uniaxially pressed under a relatively light pressure at ≈323 K for 1 min and then subjected to firing under air at 1773 K for 4 h. The two YSZ porous layers at both sides of the dense YSZ electrolyte are estimated to present a porosity of about 65% on the basis of weight changes after immersion in water [28]; the thus obtained disc is of ca. 10 mm diameter with about 5 mm diameter for the concentric porous layers.

As mentioned, a method based on impregnation of the active elements of the electrodes was employed to deposit them on the YSZ porous layers [15]. First, for the cathode ($La_{0.8}Sr_{0.2}FeO_{3-\delta}$ − LSF −) an aqueous solution of the corresponding nitrate salts, at required stoichiometry, was infiltrated to the corresponding porous layer, followed by calcination under air at 723 K. This step was repeated until the loading was 50 wt. % LSF, calcining the wafer finally at 1173 K, a temperature chosen on the basis of achieving as low as possible polarization resistance in the LSF cathode [29]. The same procedure was followed for incorporating the anode material to the corresponding YSZ porous layer by means of impregnating several times, every time followed by calcination under air at 723 K until achievement of the required weight (40 wt. %). The impregnating medium was in this case a reverse microemulsion in whose aqueous phase copper, nickel and cerium nitrate salt precursors were dissolved; full components of such microemulsion are detailed elsewhere [22]. Amounts of copper, nickel and cerium were chosen to achieve 40 wt. % of Cu + Ni (with Cu/Ni atomic ratio of 1.0) oxides, the rest being CeO_2, as reported elsewhere [22]. As mentioned, calcination temperature for the anode material was 723 K, which was observed to be sufficient to eliminate microemulsion residues, *vide infra*, as well as to get the oxides of the anode elements, as shown in previous work on similar type of materials and on the basis of separate thermogravimetric analysis [30,31]. An optical microscope sectional view of the cell which illustrates respective thickness of its components is shown in Fig. 1. Current collectors (0.25 mm gold wires) were fitted to both electrodes using gold paste (Heraeus) and subjecting the ensemble to heating in an oven at 393 K for 30 min. Finally, the cell with an

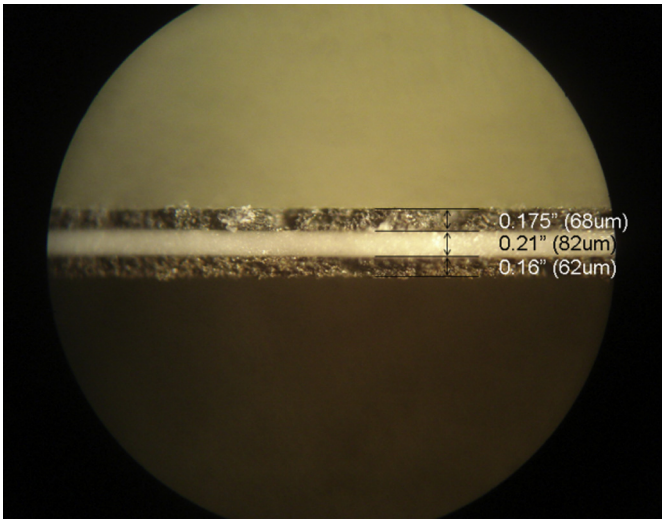

Fig. 1. Sectional view of the cell obtained by optical microscopy and illustrating the thickness of its components (top: cathode; bottom: anode).

active area of 0.35 cm^2 was sealed to one of the extremes of an alumina cylindrical tube using a refractory cement (Arenco Ceramabond 552), while the other extreme was coupled with Swagelok fittings connected to the gas handling system; a thermocouple was driven along the outer face of the alumina tube to a position close to the cell.

Electrochemical activity tests were performed with Autolab equipment (PGSTAT 30 with module FRA2 from Eco Chemie). I–V curves were measured by means of linear sweep voltammetry at a rate of 1 mV s^{-1}. Complex impedance measurements (IS spectroscopy) were made under open circuit conditions using a signal of 5 mA in a range of frequencies between 1 MHz and 10 mHz. Gases fed to the cell (either pure dry H_2 or CH_4; 50 mL min^{-1} flow) were of high purity and supplied by Air Liquide. The anodic part of the cell was preactivated by treatment under H_2 flow (50 mL min^{-1}) at 973 K. The cathode part was tested in any case under static atmospheric air. Scanning electron microscopy (SEM) pictures were taken with a Hitachi-S-2500 microscope.

3. Results and discussion

Fig. 2 displays the XRD pattern of the CuNi–CeO_2 sample prepared separately using the same synthesis parameters as employed for the SOFC anode (i.e. microemulsion preparation and final calcination at 723 K). Diffraction peaks attributable to the cubic fluorite phase of CeO_2 are observed along with several peaks related with the presence of NiO and CuO phases. The presence of broad peaks in the diffractogram indicates small crystal sizes. The XRD information confirms that the temperature employed for the preparation is enough to eliminate microemulsion residues and to get the corresponding oxides, as previously detected for the same type of formulation calcined at higher temperature [22].

Fig. 3 shows a high magnification SEM image of the microstructure of the as-prepared single cell. It shows that with CuNi–CeO_2 precursor microemulsion infiltration and subsequent calcination up to 723 K, a thin catalyst film (ca. 50–200 nm), which fully covers the whole YSZ backbone structure, is formed.

Fig. 4 displays the electrochemical behavior of the cell during reference tests performed using H_2 as fuel. As expected, the open circuit voltage (OCV) slightly decreases with increasing the operating temperature and yields values close (somewhat lower) to

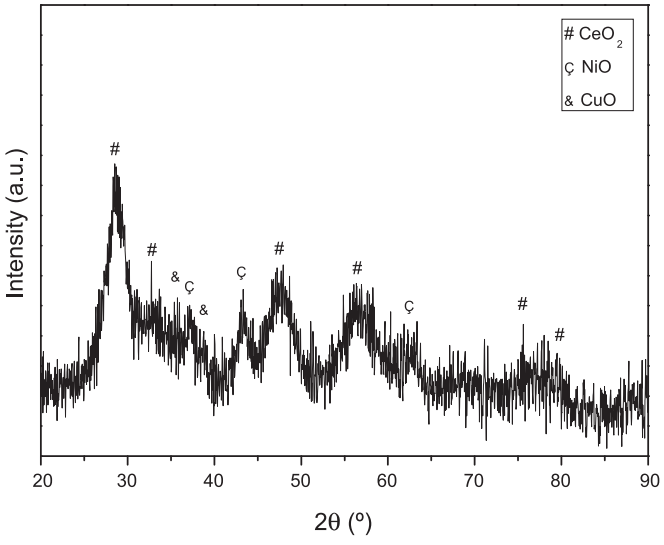

Fig. 2. X-ray diffractograms of the CuNi–CeO_2 catalyst after calcinations up to 723 K. Peaks corresponding to fluorite CeO_2 (#), NiO (Ç) and CuO (&) phases are indicated.

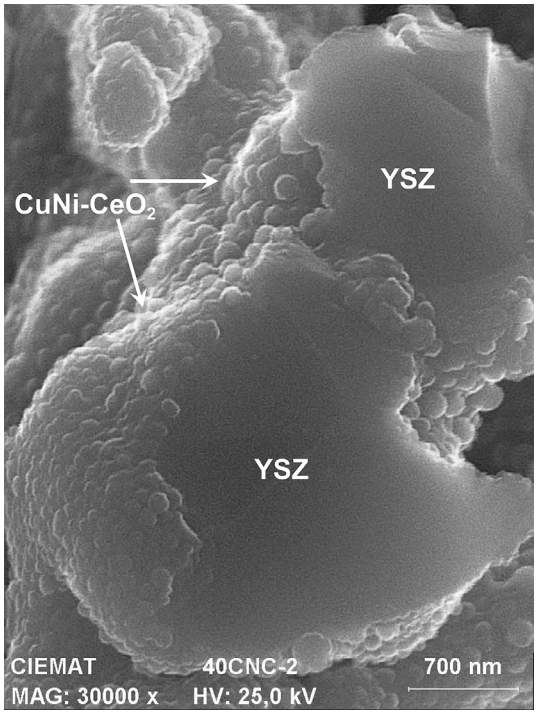

Fig. 3. Cross-sectional SEM image of YSZ backbone infiltrated with CuNi–CeO_2 precursor microemulsion (see main text), followed by calcination up to 723 K.

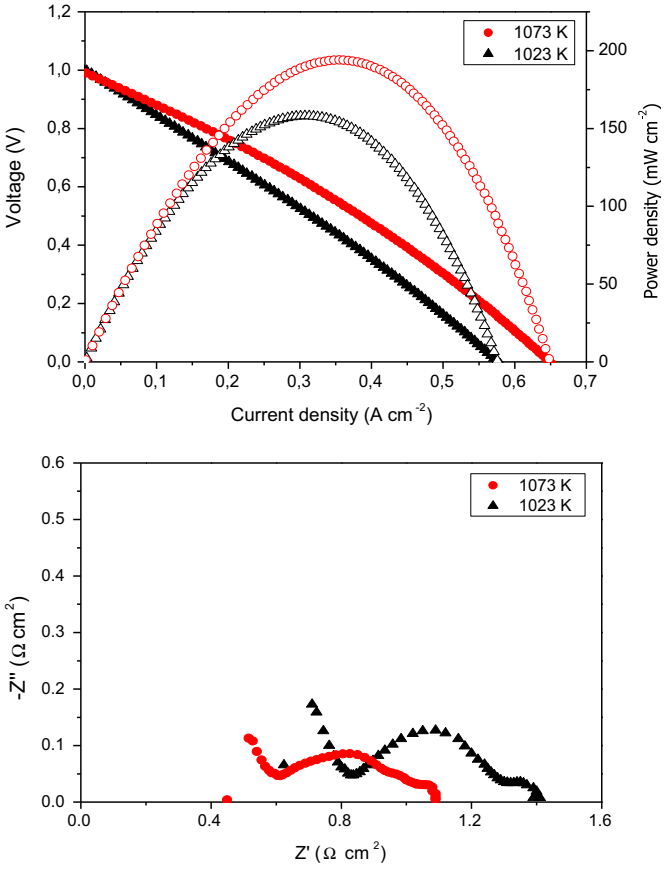

Fig. 4. Top: I–V and power density curves for the Cu–Ni–CeO_2/YSZ/LSF cell using H_2 as fuel and as a function of operating temperature. Bottom: Impedance spectra of the Cu–Ni–CeO_2/YSZ/LSF cell recorded after respective voltage measurements shown in top plot.

those predicted by the Nernst equation [4]. OCV values of the cell under dry H_2 and static air were 1.02 and 1.00 V at 1023 and 1073 K, respectively; as mentioned, both are lower than theoretical values. This could be probably due to gas leakage across the electrolyte and/or the diffusion of transitions metals cations (e.g. Cu and Ni) from electrodes into electrolyte layer. It must be noted in this sense that although low concentrations of transition metal cation in YSZ can help in improving the oxide-ion conductivity without significantly decreasing the oxide-ion transference number [32], larger concentrations can cause significant hole conduction and reduce OCV [33]. In this respect, slightly lower OCV values were also observed by Shung-Ik et al. [19] in cells prepared by impregnation with $Cu_{0.8}Ni_{0.2}$–CeO_2 and $Cu_{0.7}Ni_{0.3}$–CeO_2 as anodes although such behavior was not detected in cells with anodes of Cu–CeO_2 and $Cu_{0.95}Ni_{0.05}$–CeO_2. They explained such observation as probably due to the formation of microcracks in the electrolyte after thermal treatment under *n*-butane. On the other hand, Guo et al. [34], and Li and Barnett [35], also observed relatively low OCV values when using cells with interfaces of LSGM/LDC using NiO–$Sm_{0.2}Ce_{0.8}O_{2-\delta}$ and NiO–$La_{0.4}Ce_{0.6}O_{2-\delta}$ as anode, respectively, and suggested that the lower OCV values were caused by diffusion of cations in the electrolyte films. It must be noted in this sense that both YSZ and LSGM are electrolytes with only ionic conductivity. In addition, the use of static air as oxidant instead of an oxygen flow could also affect to the decrease of the OCV value.

An increase in the cell power with operating temperature is most likely related to the increase in the electrolyte ionic conductivity as well as electrode activity. This is reflected by IS spectra shown in Fig. 4, which were taken immediately after the corresponding voltage measurements displayed in the same Figure (top plot). Ohmic resistance values extracted from the spectra were of 0.72 and 0.50 Ω cm^2 close to those expected for YSZ electrolyte of about 100 μm thickness, based on experimental calculations. The first contribution appearing at high frequencies could be related with the impedance in the grain border [36]. In turn, the other two arcs basically observed in the Nyquist diagrams of Fig. 4 reflect polarization resistances of about 0.69 Ω cm^2 and 0.61 Ω cm^2 at 1023 and 1073 K, respectively. The impedance data (disregarding grain border contribution) of Fig. 4 were fitted to an equivalent circuit of the type $R_o(R_1Q_1)(R_2Q_2)(R_3Q_3)$ using ZView software. R_o is the ohmic resistance of the cell (mainly associated with electrolyte), and three series connected elements (RQ) describe the processes associated with cathode–electrolyte interface and anode–electrolyte interface. R is a resistance and Q is a constant phase element representing time-dependent capacitive elements. Parameters extracted from this are the relaxation frequency through $\omega_o = (RQ)^{-1/n}$ which in turn depends on the true capacitance – $\omega_o = 1/(RC)$ –, expressed as [37]:

$$C = R^{(1-n)/n}Q^{1/n}$$

Corresponding fitted results of resistance, capacitance and relaxation frequency are collected in Table 1. It is observed that mid frequency contributions appear and increase with the temperature, corresponding to capacitance values around 10^{-3} F cm^{-2}; these may be related to phenomena affecting the electrochemical reaction at the triple phase boundary (TPB) [4,38]. On the other hand, at low frequencies ($\approx 10^{-1}$ Hz), there appears a process with relatively high capacitance. Such high capacitance is not attributable to interfacial or surface processes but to material bulk ones [39]. They could be related to chemical capacitance processes appearing in mixed conductors which have been associated to variations in the chemical composition of the electrodes upon application of a voltage [40]. Thus, such high capacitance could be related to changes in the electrode stoichiometry as a consequence of oxygen transfer processes under anodic reaction conditions [34].

Table 1
Resistance (R), capacitance (C) and relaxation frequency (f) obtained from equivalent circuit simulation of IS spectra shown in Fig. 3.

Temperature (K)	R (Ω cm^2)	C (F cm^{-2})	f (Hz)
1023	0.46	8.61×10^{-4}	4.04×10^{2}
	0.19	4.05×10^{-3}	2.06×10^{2}
	0.05	3.32×10^{1}	1.06×10^{-1}
1073	0.55	7.85×10^{-4}	3.70×10^{2}
	0.04	1.69×10^{-2}	2.29×10^{2}
	0.02	3.98×10^{1}	1.63×10^{-1}

Fig. 5 shows the effect of temperature on I–V curves and power density produced by the cell when operating under pure dry CH_4 and static air. First to be noted, OCV values obtained were 0.94 and 1.00 V at 1023 and 1073 K. The increase in OCV values with increasing temperature is opposite to the trend observed when using hydrogen as fuel (Fig. 4). In this sense, it is known that information on the operating anode reaction can be obtained from OCV measurements [41]. However, unfortunately, interpretation of the OCV values when fueling with methane is always more complicated because of the likelihood of different alternative routes for methane oxidation. As the pure methane enters the anode of SOFCs, H_2, CO, CO_2 and H_2O can be formed by partial electrochemical oxidation of methane and direct electrochemical oxidation of methane. In addition, deposited carbon can be formed by methane decomposition on this type of anodes [22,24–26]. On the whole, various chemical and electrochemical reactions may take place among the different reactants and products as well as with O^{2-} electrochemically transferred to the anode. The electrochemical reactions are listed next [42,43]:

$$CH_4 + 4O^{2-} \rightarrow CO_2 + 2H_2O + 8e^- \quad (1)$$

$$CH_4 + 2O^{2-} \rightarrow CO_2 + 2H_2 + 4e^- \quad (2)$$

$$H_2 + O^{2-} \rightarrow H_2O + 2e^- \quad (3)$$

$$CO + O^{2-} \rightarrow CO_2 + 2e^- \quad (4)$$

$$C + O^{2-} \rightarrow CO + 2e^- \quad (5)$$

Additionally, chemical reactions, as listed below, may also take place

$$CH_4 \rightarrow C + 2H_2 \quad (6)$$

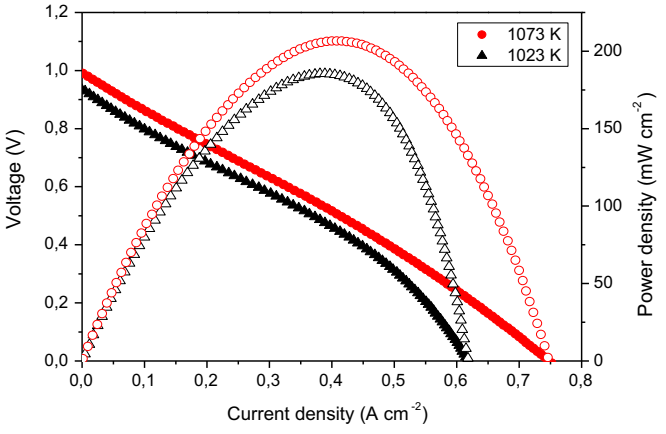

Fig. 5. I–V and power density curves for the Cu–Ni–CeO_2/YSZ/LSF cell using pure dry CH_4 as fuel and as a function of operating temperature.

$$CH_4 + H_2O \rightarrow CO + 3H_2 \quad (7)$$

$$CO + H_2O \rightarrow CO_2 + H_2 \quad (8)$$

$$CH_4 + CO_2 \rightarrow 2CO + 2H_2 \quad (9)$$

$$2CO \rightarrow C + CO_2 \quad (10)$$

$$C + H_2O \rightarrow CO + H_2 \quad (11)$$

In this sense, the evolution of OCV values with the operating temperature when using CH_4 as fuel could be related to the relative contribution of the mentioned reactions at each temperature which would determine the gas phase composition at the TPB in each case [41]; the observed increase of OCV with the operating temperature when using dry methane as fuel suggests in this sense a predominance of partial oxidation electrochemical reaction in the process, equation (2) [41,44]. In any case, experimental OCV values appear lower than theoretical ones [4,41], presumably due, as pointed out above when using H_2 as fuel, to the presence of small gas leaks and/or to the diffusion of transition metals cations into the electrolyte layer, as well as because of the use of static air as oxidant. On the other hand, it can be observed that both I–V curves in Fig. 5 display similar slope except at high current density at which concentration losses apparently appear at 1023 K which are eliminated upon

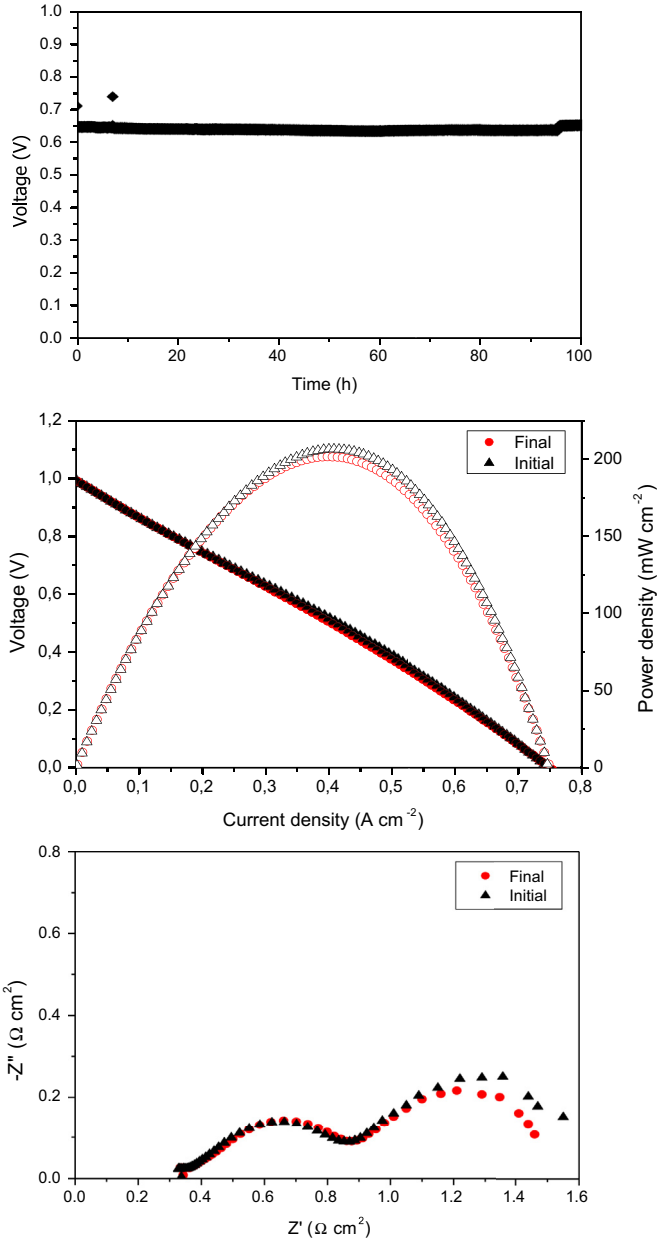

Fig. 6. Top: Load test performed at 100 mA and 1073 K during 100 h under pure dry methane over the Cu–Ni–CeO_2/YSZ/LSF cell. I–V and power density curves (middle) and IS spectra (bottom) for the Cu–Ni–CeO_2/YSZ/LSF cell using pure dry CH_4 as fuel before and after the durability test shown in top plot.

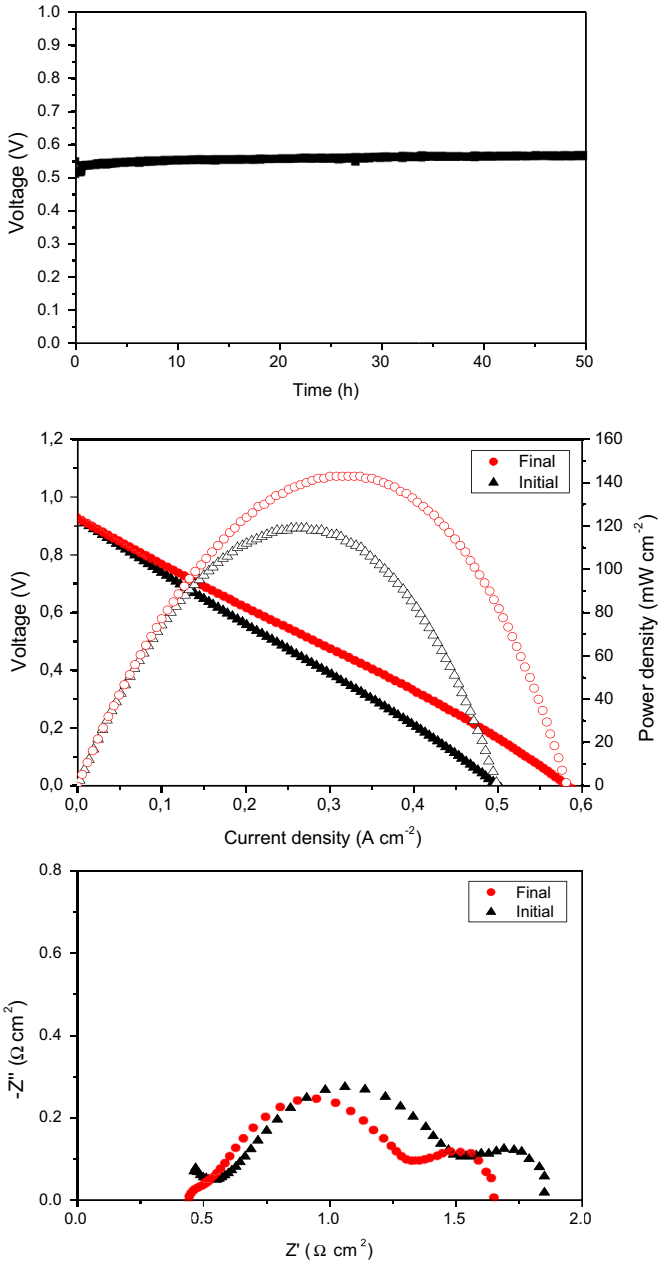

Fig. 7. Top: Load test performed at 84 mA and 1023 K during 50 h under pure dry methane over the Cu–Ni–CeO_2/YSZ/LSF cell. Middle: I–V and power density curves for the Cu–Ni–CeO_2/YSZ/LSF cell using pure dry CH_4 as fuel before and after the test shown in top plot. Bottom: Impedance spectra of the Cu–Ni–CeO_2/YSZ/LSF cell performed after recording of I–V curves displayed in middle plot.

Table 2
Resistance (R), capacitance (C) and relaxation frequency (f) obtained from equivalent circuit simulation analysis of IS spectra in Fig. 7.

IS spectrum	R (Ω cm^2)	C (F cm^{-2})	f (Hz)
Initial	0.17	4.33×10^{-5}	2.10×10^{4}
	0.89	3.21×10^{-3}	5.55×10^{1}
	0.36	4.57×10^{0}	9.56×10^{-2}
Final	0.09	7.74×10^{-5}	2.29×10^{4}
	0.89	3.28×10^{-3}	6.08×10^{1}
	0.34	4.66×10^{-0}	9.90×10^{-2}

increasing the temperature. This suggests that carbon deposition, formed as a consequence of the interaction of the anode material with methane at this temperature, could be affecting access of the fuel to the TPB as well as producing mass transport problems.

In any case, the electrochemical behavior appears rather stable at 1073 K, as confirmed by the durability test shown in Fig. 6, performed at the intensity required to achieve about 90% of the maximum power, in which no deactivation is apparently produced during the course of the 100 h test. This is confirmed by similarities observed in both I–V curves and IS spectra recorded before and after the durability test (Fig. 6), which reveal that only a small decrease of the cell activity is produced during the course of the test.

Following tests under CH_4 at 1073 K, the temperature was decreased to 1023 K and the anode part was treated under H_2 for 1 h aiming to clean any possible carbon deposits that could remain after the tests at 1073 K. However, an important activity decrease was observed in the cell upon recording corresponding I–V curve with respect to tests performed previously under the same operating conditions. Thus, maximum power density of about 120 mW cm^{-2} at 0.25 A cm^{-2} was achieved this time, apparently lower than detected previously (Fig. 5). Such deactivation is most likely related to further sintering, produced during first stages of the tests at 1073 K, of the active CuNi alloy particles likely present under the employed operating conditions [22]. In any case, a load test during 50 h under pure dry CH_4 shows the stability of the cell under such conditions too (Fig. 7). Furthermore, a small increase in the obtained voltage is produced which indicates that a certain reactivation of the cell has been produced during the course of the test in Fig. 7. This is confirmed by comparing I–V curves obtained before and after such test, as shown in Fig. 7. Corresponding IS spectra are displayed in Fig. 7 and values for the various components of equivalent circuits obtained upon corresponding simulation analysis are collected in Table 2. The main difference is related to the appreciable decrease in the resistance of the process at ca. 2×10^4 Hz with associated capacitance in the range of 4–8×10^{-5} F cm^{-2}. Such behavior can be related with an enhancement in the interconnection of metallic zones as a consequence of formation of carbon deposits under these conditions which would act as bridges between the CuNi alloy particles while basically keeping electrochemical reaction conditions at the TPB, according to data extracted from the simulation (Table 2). A similar phenomenon of cell activity enhancement as a consequence of formation of a small amount of carbon deposits was previously proposed by Kim et al. during a study of a cell with an anode composed by Cu–Ni (with Cu/Ni ratio of 4.0) in combination with CeO_2, suggesting there could exist at the anode more or less isolated metallic regions not contributing strongly to the electrochemical reaction and whose electrical interconnection as well as with the external circuit would be enhanced by carbon deposition [45,46]. This is as well reflected in a decrease of both ohmic resistance (from about 0.46 to 0.44 Ω cm^2) and the resistance associated with this phenomenon (from 0.17 to 0.09 Ω cm^2) according to direct analysis of the arcs in the IS spectra (Fig. 7). We cannot however discard that the observed enhancement in the electrochemical performance under CH_4 at 1023 K (Fig. 7) is related rather to a gradual decrease in the amount of deposited carbon during the course of the test as a consequence of reactions (5) and (11) exposed above. It must be noted in this sense and in comparative terms that the amount of carbon deposits formed depends in principle on the specific current density employed in each case while H_2O presence could have also detrimental effects since nickel oxidation can be also favored [44,47].

In definitive, the fabricated cell having an anode based on combination of Cu–Ni (at 1:1 atomic ratio) with CeO_2 (on the basis of previous characterization of a similar separate anode with the same formulation as used here and prepared by the same microemulsion based method [22], as well as XRD characterization, Fig. 2), has been shown to be able to directly oxidize pure dry CH_4 in a rather stable way at 1073 K. Some instability is evidenced to appear at the lowest temperature employed (1023 K). This is attributed to formation of carbon deposits which, in this case, favorably affect to the cell activity. Certainly the difference observed with respect to the operating temperature must be related with differences in oxygen transport rates through the cell, and in particular through the anode portion, which limit oxidation

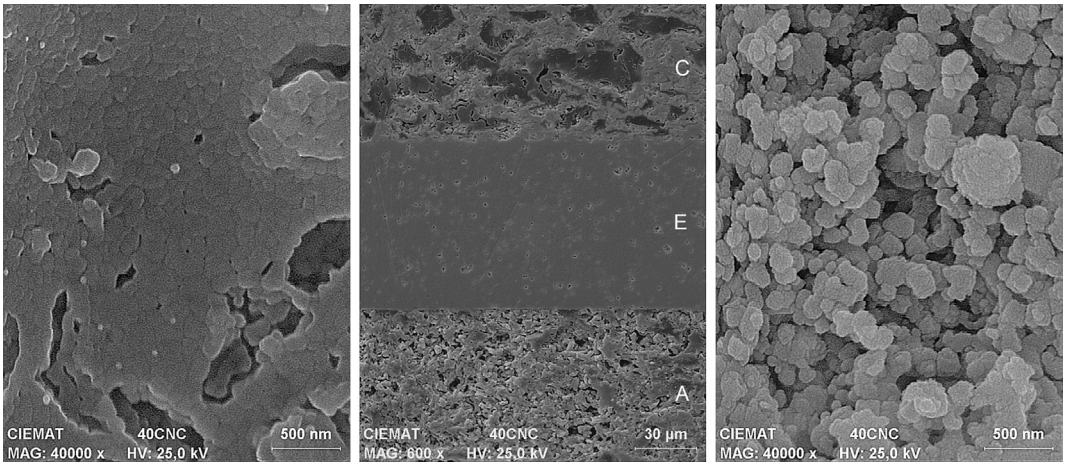

Fig. 8. SEM pictures of the cathode (left), sectional view of the full cell (C: cathode, E: electrolyte, A: anode; middle) and anode (right) of the Cu–Ni–CeO_2/YSZ/LSF cell after completion of electrochemical tests indicated in main text.

reaction at the anode as the temperature decreases, thus favoring incomplete oxidation of CH_4 (and/or $C + H_2$ formed upon interaction of CH_4 with the CuNi alloy most likely present [22]). Further analysis of the anode microstructure under reaction conditions would however be certainly required to determine differences with other systems in the literature with related formulations [4,16,21]; note in this sense that stable behavior under direct methane oxidation conditions is difficult to attain with the relatively high Ni/Cu ratio here employed [16], being typically required the use of additives, like for instance Ba, to increase the anode stability [21].

A final qualitative exploration of the cell microstructure at the end of the presented electrochemical tests has been performed by SEM microscopy. As shown in Fig. 8, the cathode apparently presents a good particle interconnection while the anode appears as more granular and porous. This latter structure would favor the presence of mentioned more or less isolated metallic regions serving as connection to the external circuit but not strongly involved in TPB reactions, which would favor overall activity of the cell by enhancing electrical contacts at the anode.

4. Conclusions

A Cu–Ni–CeO_2/YSZ/LSF SOFC for direct oxidation of CH_4 has been prepared in which the electrodes were deposited by impregnation, employing a reverse microemulsion as impregnating medium in the case of the anode. The latter must be basically composed by Cu–Ni in combination with CeO_2, according to XRD analysis and in agreement with recent characterization [22], and with porous YSZ acting as support. The electrochemical performance either under H_2 or pure dry CH_4 has been evaluated at 1023–1073 K and complementary electrochemical characterization by IS has been also performed. The results evidence the ability of the cell to perform efficiently under CH_4 with an electrochemical behavior which apparently depends on the operating temperature. While a stable behavior is observed when operating during 100 h at 90% maximum power conditions at 1073 K, a small increase in the cell activity is observed with time at 1023 K. The latter is ascribed to possible formation of carbon deposits as a consequence of the lower oxidation activity at the anode possibly due to oxygen transport limitations at such temperature. As previously proposed and on the basis of IS results, such deposits could result beneficial for the anode microstructure by enhancing electrical contacts in it and with the external circuit without strongly affecting to the TPB region.

Acknowledgments

A.H. thanks the Ministerio de Educación y Ciencia (MEC) for an FPU Ph.D. grant under which his contribution to this work was done. Thanks are due to the Comunidad de Madrid (project DIVERCEL S2009/ENE-1475) for financial support. Support from EU COST CM1104 action is also acknowledged. Thanks are due to Prof. R.J. Gorte of the Department of Chemical and Biomolecular Engineering at the University of Pennsylvania (USA) for the help provided, during a stay of A.H. in his laboratory, with respect to various aspects related to the fabrication of the single cells.

References

[1] B.C.H. Steele, A. Heinzel, Nature 414 (2001) 345–352.
[2] B.C.H. Steele, J. Mater. Sci. 36 (2001) 1053–1068.
[3] J.M. Ralph, A.C. Schoeler, M. Krumpelt, J. Mater. Sci. 36 (2001) 1161–1172.
[4] S. McIntosh, R.J. Gorte, Chem. Rev. 104 (2004) 4845–4865.
[5] K. Sasaki, Y. Teraoka, J. Electrochem. Soc. 150 (2003) A878–A884.
[6] E.P. Murray, T. Tsai, S.A. Barnett, Nature 400 (1999) 649–651.
[7] S. Park, R.J. Gorte, J.M. Vohs, Appl. Catal. A 200 (2000) 55–61.
[8] A.-L. Sauvet, J. Fouletier, J. Power Sources 101 (2001) 259–266.
[9] N.M. Galea, D. Knapp, T. Ziegler, J. Catal. 247 (2007) 20–33.
[10] R.J. Gorte, J.M. Vohs, J. Catal. 216 (2003) 477–486.
[11] S. Park, R. Craciun, J.M. Vohs, R.J. Gorte, J. Electrochem. Soc. 146 (1999) 3603–3605.
[12] S. Park, J.M. Vohs, R.J. Gorte, Nature 404 (2000) 265–267.
[13] H. Kim, S. Park, J.M. Vohs, R.J. Gorte, J. Electrochem. Soc. 148 (2001) A693–A695.
[14] R.J. Gorte, H. Kim, J.M. Vohs, J. Power Sources 106 (2002) 10–15.
[15] S. Jung, C. Lu, H. He, K. Ahn, R.J. Gorte, J.M. Vohs, J. Power Sources 154 (2006) 42–50.
[16] R.J. Gorte, J.M. Vohs, Curr. Opin. Coll. Interf. Sci. 14 (2009) 236–244.
[17] C. Sun, U. Stimming, J. Power Sources 171 (2007) 247–260.
[18] Z. Xie, W. Zhu, B. Zhu, C. Xia, Electrochim. Acta 51 (2006) 3052–3057.
[19] S.I. Lee, J.M. Vohs, R.J. Gorte, J. Electrochem. Soc. 151 (2004) A1319–A1323.
[20] E.W. Park, H. Moon, M. Park, S.H. Hyun, Int. J. Hydr. Ener. 34 (2009) 5537–5545.
[21] D. La Rosa, A. Sin, M. Lo Faro, G. Monforte, V. Antonucci, A.S. Aricò, J. Power Sources 193 (2009) 160–164.
[22] A. Hornes, P. Bera, M. Fernandez-Garcia, A. Guerrero-Ruiz, A. Martínez-Arias, Appl. Catal. B 111–112 (2012) 96–105.
[23] S. Eriksson, U. Nylén, S. Rojas, M. Boutonnet, Appl. Catal. A 265 (2004) 207–219.
[24] A. Hornes, D. Gamarra, G. Munuera, J.C. Conesa, A. Martínez-Arias, J. Power Sources 169 (2007) 9–16.
[25] A. Hornés, D. Gamarra, G. Munuera, A. Fuerte, R.X. Valenzuela, M.J. Escudero, L. Daza, J.C. Conesa, P. Bera, A. Martínez-Arias, J. Power Sources 192 (2009) 70–77.
[26] A. Hornes, G. Munuera, A. Fuerte, M.J. Escudero, L. Daza, A. Martinez-Arias, J. Power Sources 196 (2011) 4218–4225.
[27] P. Blennow, K.K. Hansen, L.R. Wallenberg, M. Mogensen, ECS Trans. 13 (26) (2008) 181–194.
[28] G. Kim, J.M. Vohs, R.J. Gorte, J. Mater. Chem. 18 (2008) 2386–2390.
[29] W. Wang, M.D. Gross, J.M. Vohs, R.J. Gorte, J. Electrochem. Soc. 154 (2007) B439–B445.
[30] A. López Camara, A. Kubacka, Z. Schay, Zs. Koppany, A. Martínez-Arias, J. Power Sources 196 (2011) 4364–4369.
[31] A. Hornés Martínez, PhD Thesis, Universidad Autónoma de Madrid, 2010.
[32] V.V. Khartona, A.P. Viskup, A.A. Yaremchenko, R.T. Baker, B. Gharbage, G.C. Mather, F.M. Figueiredo, E.N. Naumovich, F.M.B. Marques, Solid State Ionics 132 (2000) 119–130.
[33] T. Ishihara, T. Shibayama, M. Honda, H. Nishiguchi, Y. Takita, J. Electrochem. Soc. 147 (4) (2000) 1332–1337.
[34] W. Guo, J. Liu, Y. Zhang, Electrochim. Acta 53 (2008) 4420–4427.
[35] Y. Li, S.A. Barnett, Electrochem. Solid-State Lett. 9 (6) (2006) A285–A288.
[36] J.T.S. Irvine, D.C. Sinclair, A.R. West, Adv. Mater. 2 (1990) 132–138.
[37] E. Chinarro, J.R. Jurado, F.M. Figueiredo, J.R. Frade, Solid State Ionics 160 (2003) 161–168.
[38] P. Vernoux, M. Guillodo, J. Fouletier, A. Hammou, Solid State Ionics 135 (2000) 425–431.
[39] Q.X. Fu, F. Tietz, D. Stöver, J. Electrochem. Soc. 153 (2006) D74–D83.
[40] J. Jamnik, J. Maier, Phys. Chem. Chem. Phys. 3 (2001) 1668–1678.
[41] K. Kendall, C.M. Finneryy, G. Saunders, J.T. Chung, J. Power Sources 106 (2002) 323–327.
[42] H. You, A. Abuliti, X. Ding, Y. Zhou, J. Power Sources 165 (2007) 722–727.
[43] X. Zhang, S. Ohara, H. Chen, T. Fukui, Fuel 81 (2002) 989–996.
[44] M.A. Buccheri, A. Sing, J.M. Hill, J. Power Sources 196 (2011) 968–976.
[45] H. Kim, C. Lu, W.L. Worrell, J.M. Vohs, R.J. Gorte, J. Electrochem. Soc. 149 (2002) A247–A250.
[46] Z.H. Bi, J.H. Zhu, Electrochem. Solid-State Lett. 12 (2009) B107–B111.
[47] G. Chen, G. Guan, H.X. You, A. Abudula, J. Power Sources 196 (2011) 6022–6028.